Magnetoresistivity and Monte Carlo studies of magnetic phase transitions in C_6Eu

S. T. Chen and M. S. Dresselhaus
Department of Physics, Massachusetts Institute of Technology, Cambridge, Massachusetts 02139

G. Dresselhaus
Francis Bitter National Magnet Laboratory, Massachusetts Institute of Technology, Cambridge, Massachusetts 02139

H. Suematsu, H. Minemoto, and K. Ohmatsu
Institute of Materials Science, University of Tsukuba, Sakura, Ibaraki 305, Japan

Y. Yosida
Department of Physics, Toyama University, Toyama 930, Japan
(Received 2 January 1986)

The high-field magnetoresistivity $\rho(H)$ of the antiferromagnetic first-stage graphite intercalation compound C_6Eu has been measured with $\mathbf{H}\perp\hat{\mathbf{c}}$ and $\mathbf{H}\|\hat{\mathbf{c}}$. Both the longitudinal ($\mathbf{J}\|\mathbf{H}$) magnetoresistivity $\rho_l(H_\perp)$ and the transverse ($\mathbf{J}\perp\mathbf{H}$) magnetoresistivity $\rho_t(H_\perp)$ with $\mathbf{H}\perp\hat{\mathbf{c}}$ show distinct changes across the magnetic phase boundaries which occur at fields of 1.5, 8, 15, and 21.5 T at a temperature $T=4.2$ K. The phase transition at $H=15$ T was not observed previously by the pulsed magnetization measurements. A Monte Carlo simulation based on the Hamiltonian of Sakakibara and Date was carried out for the C_6Eu system. The 15-T phase transition is explained as a transition from a "canted" to a "fan" state. The transverse magnetoresistivity $\rho_t(H_\|)$ with $\mathbf{H}\|\hat{\mathbf{c}}$ shows a clear anomaly at the field corresponding to the onset of the transition to the spin-aligned paramagnetic state. A magnetic phase diagram has been accurately determined based on the results of the magnetoresistivity measurements. The various spin configurations in the phase diagram are identified and the parameters of the Hamiltonian are determined using the results of the Monte Carlo simulation.

I. INTRODUCTION

C_6Eu is a stage-1 graphite intercalation compound (GIC) based on the rare-earth magnetic metal Eu. In the intercalation compound, the europium atoms are located over the centers of graphite hexagons and form a $(\sqrt{3}\times\sqrt{3})R30°$ superlattice, with a planar triangular lattice commensurate to the graphite honeycomb planes.[1,2] Each Eu atom has six in-plane nearest neighbors at 4.31 Å and six next-nearest neighbors at 5.47 Å on adjacent Eu layers. The second-nearest-neighbor in-plane distance is 7.465 Å. If we neglect the graphite layers, the Eu atoms form a hexagonal close-packed structure with $\alpha\beta$ stacking order.[2]

The magnetic properties of the C_6Eu compound have been studied extensively.[3–8] The paramagnetic susceptibility[4] and Mössbauer experiments[5] establish that the Eu is in the divalent Eu^{2+} state with $S=\frac{7}{2}$, $L=0$, and $J=S$. The two Eu valence electrons are transferred to the graphite π bands. The in-plane electrical resistivity of C_6Eu at 4.2 K is $\rho_\perp\sim10^{-6}\Omega$ cm, while the value $\rho_\|$ is two orders of magnitude larger along the c axis.[6] Thus, C_6Eu is a highly anisotropic quasi-two-dimensional conductor. The magnetic susceptibility of C_6Eu shows Curie-Weiss behavior above 40 K, and an antiferromagnetic ordering is observed below the Néel temperature ($T_N=40$ K).[4] Some of the pertinent magnetic parameters are listed in Table I. C_6Eu is a highly anisotropic XY-like magnetic system with antiferromagnetic in-plane nearest-neighbor interaction and ferromagnetic interplanar interactions.[7]

The Eu intercalant acts as a donor in graphite intercalation compounds and C_6Eu is the first donor GIC to be studied for its magnetic properties. The magnetization of C_6Eu for $\mathbf{H}\perp\hat{\mathbf{c}}$ shown in Fig. 1 was first measured by Suematsu *et al.*[1,4] using a pulsed magnetic field up to 40 T. Three critical fields ($H_{c0}=1.6$ T, $H_{c1}=6.4$ T,

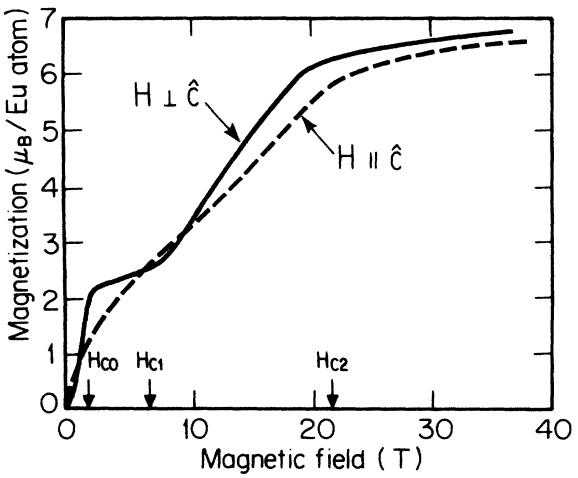

FIG. 1. Magnetization of C_6Eu at 4.2 K for the applied magnetic field parallel and perpendicular to the c axis, from the results of Suematsu *et al.* (Ref. 1) (see text).

TABLE I. Magnetic parameters for C_6Eu. (From Ref. 1.)

	$\mathbf{H}\perp\hat{\mathbf{c}}$	$\mathbf{H}\|\|\hat{\mathbf{c}}$
Néel temperature (K)	40.0±1.0	
Curie-Weiss constant (K)	1±5	3±5
Molar Curie constant (emu K/mole)	7.2±0.1	5.6±0.1
Effective paramagnetic moment (μ_B)	7.6	6.7
g-factor at 150 K (from ESR)	1.94	1.92
Saturation moment at $H=30$ T (μ_B)	6.5	6.0

$H_{c2}=21.5$ T) are identified from these data. The magnetic moment is saturated above H_{c2} with a saturation moment $\sim 6.5\mu_B$ close to the value of $7\mu_B$ expected for an $S=\frac{7}{2}$ state. Between H_{c0} and H_{c1}, an unusual metamagnetic plateau is observed with moment $\sim 2.2\mu_B$ which is $\sim\frac{1}{3}$ of the saturation moment. The magnetization between H_{c1} and H_{c2} is almost linear in field.

To explain these magnetic properties, the C_6Eu is treated as a three-dimensional (3D) XY magnetic system.[7] Qualitative agreement with experiment was obtained by choosing the interatomic exchange coupling constants "phenomenologically"[7] as antiferromagnetic for the nearest-neighbor in-plane coupling ($J_0<0$); ferromagnetic for the next-nearest-neighbor in-plane coupling ($J_1>0$) and for the nearest-neighbor interplanar coupling ($J'>0$). It was, however, found that higher-order exchange interactions were needed to explain the metamagnetism between H_{c0} and H_{c1}.[1,3,7] The Hamiltonian for the magnetic system used by Sakakibara and Date[1,3,7] to explain the magnetization results is

$$\begin{aligned}\mathscr{H}_0=&-J_0\sum_{\mathrm{NN}}\mathbf{S}_i\cdot\mathbf{S}_j-J_1\sum_{\mathrm{NNN}}\mathbf{S}_i\cdot\mathbf{S}_j-J'\sum_{\mathrm{NN}}\mathbf{S}_i\cdot\mathbf{S}_k\\&-B\sum_{\mathrm{NN}}(\mathbf{S}_i\cdot\mathbf{S}_j)^2-g\mu_B\sum_i\mathbf{S}_i\cdot\mathbf{H}\\&+K\sum_{4-\text{spin ring}}[(\mathbf{S}_i\cdot\mathbf{S}_j)(\mathbf{S}_k\cdot\mathbf{S}_l)+(\mathbf{S}_i\cdot\mathbf{S}_l)(\mathbf{S}_j\cdot\mathbf{S}_k)\\&-(\mathbf{S}_i\cdot\mathbf{S}_k)(\mathbf{S}_j\cdot\mathbf{S}_l)]\,,\end{aligned}\tag{1}$$

where the resulting parameters were evaluated from the values of the critical fields H_{c0}, H_{c1}, and H_{c2} and are listed in Table II. The first term in Eq. (1) is the antiferromagnetic in-plane nearest-neighbor exchange interaction. The second term is the ferromagnetic in-plane next-nearest-neighbor exchange interaction. The third term is the ferromagnetic interplane nearest-neighbor exchange interaction. The fourth term is the in-plane nearest-neighbor biquadratic exchange interaction. The fifth term is the Zeeman energy associated with the external magnetic field. The last term is the in-plane four-spin ring cyclic exchange interaction.[1,7]

The introduction of an interaction of the form $(\mathbf{S}_i\cdot\mathbf{S}_j)^2$ is novel, but has been reported for other systems.[9-11] In a localized spin system, the magnitude of the higher-order interactions must be small. From the magnetization data[1,7] it is also found that for C_6Eu the higher-order interaction parameters B and K are very small compared with J_0, consistent with localized Eu spins, but the large-S value ($S=\frac{7}{2}$) makes the contribution from the biquadratic and four-spin ring terms important. The spin arrangements in different phases proposed by Sakakibara and Date are (a) for $H<H_{c0}\Longrightarrow\Delta$ phase [inset to Fig. 2(a)], (b) for $H_{c0}<H<H_{c1}\Longrightarrow$ ferrimagnetic phase [inset of Fig. 2(b)], (c) for $H_{c1}<H<H_{c2}\Longrightarrow$ "canted" phase [inset of Fig. 2(c)], and (d) For $H>H_{c2}\Longrightarrow$ spin aligned paramagnetic phase (not shown). The Δ phase refers to the frustrated spin arrangement for spins on a triangular lattice with antiferromagnetic nearest-neighbor exchange. In the spin-aligned paramagnetic phase, all the spins are aligned along the magnetic field.

The results of the Monte Carlo simulations in the present work[12] are mainly in agreement with the spin arrangements proposed by Sakakibara and Date.[7] The present Monte Carlo simulations, however, indicate some refinements to their spin configurations. Firstly, their spin arrangements are strictly applicable only in the limit of zero interplanar nearest-neighbor ferromagnetic exchange coupling J' [i.e., if C_6Eu is treated as a purely two-dimensional (2D) system]. By considering a finite interplanar exchange coupling,[10] the Monte Carlo simulation shows that the canted phase mentioned above will split into two different phases, consistent with the magnetoresistivity measurements for C_6Eu also reported in this work. A preliminary report of the magnetoresistivity measurements was previously given.[13] Figure 1 also shows the magnetization curve for $\mathbf{H}\|\hat{\mathbf{c}}$. The $\frac{1}{3}$ moment plateau does not appear for this magnetic field orientation and the magnetization curve is nearly linear in field. A comparison between the magnetization and magnetoresis-

TABLE II. Parameters for magnetic interactions in C_6Eu.

	J_0 (K)	J_1 (K)	J' (K)	BS^2 (K)	KS^2 (K)
Sakakibara and Date model[a]	−0.5	0.4	0.1	0.02	0.05
Monte Carlo simulation	−0.656	0.525	0.131	0.0262	0.0656

[a]From Ref. 7.

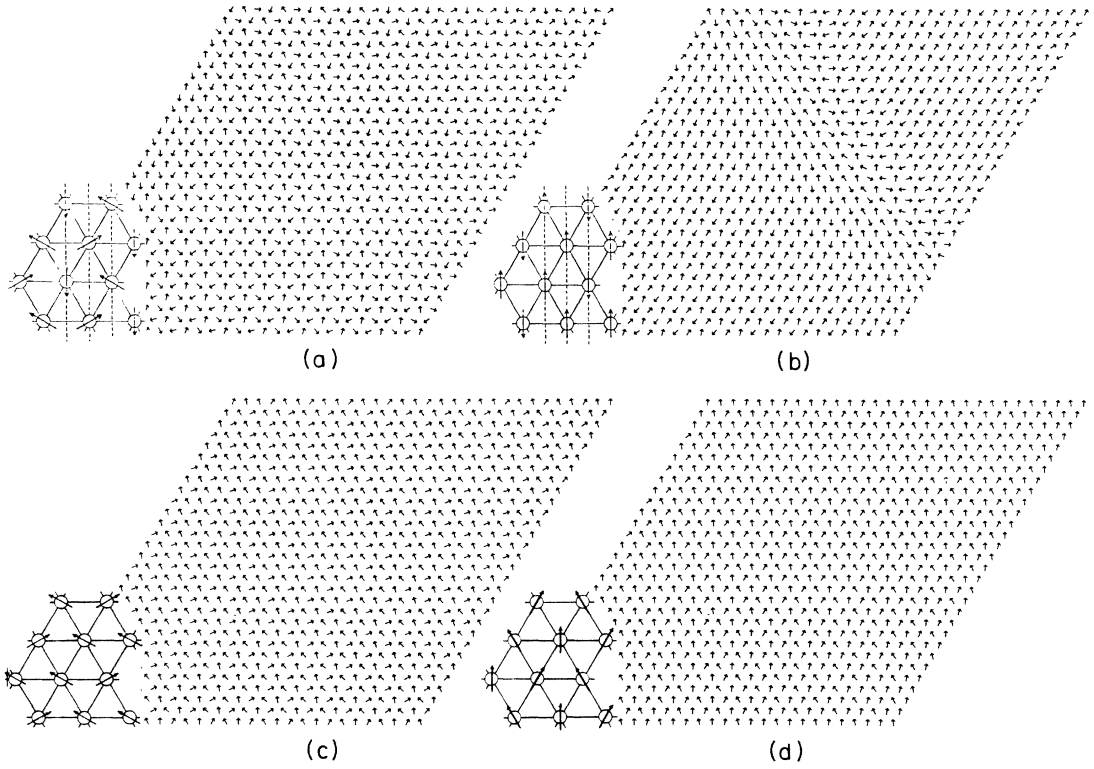

FIG. 2. Spin configurations of a plane of 30×30 spins for Eu ions in C_6Eu obtained from the Monte Carlo simulation, showing (a) Δ state at $H=0$, (b) ferrimagnetic phase at $H=3$ T, (c) "canted" phase at $H=13$ T, and (d) "fan" phase at $H=17$ T. The spin-aligned paramagnetic phase above H_{c2} where all spins are aligned along the field is not shown (see text).

tance measurements for the orientation $\mathbf{H}||\hat{\mathbf{c}}$ is also presented in this work.

The in-plane resistivity of C_6Eu is $\sim 50\ \mu\Omega$ cm at room temperature,[1] which is very large compared with that of stage-1 Li-GIC (C_6Li) which has the same in-plane structure.[14] This difference is attributed to the extraordinarily large electron scattering associated with spin fluctuations.[15] At low temperature (4.2 K) where the system is magnetically ordered, the resistivity is $\sim 3\ \mu\Omega$ cm, which is comparable with that of other stage-1 compounds based on nonmagnetic metal intercalants.[14] Since the resistivity below T_N is strongly affected by spin fluctuations, the magnetoresistance will be sensitive to magnetic phase transitions in C_6Eu. This effect was first observed both in the temperature and magnetic-field-dependent measurements of the resistivity of C_6Eu,[1] performed in the low-field ($H<10$ T) region.[16] The present work describes recent magnetoresistence measurements for magnetic fields up to 29 T (Ref. 13) and the magnetic phase diagram based on these measurements for $\mathbf{H}\perp\hat{\mathbf{c}}$ is presented. Monte Carlo simulations are used to identify the spin configurations for the various magnetic phases, to investigate the role of J' (the nearest-neighbor interplanar exchange interaction) and H_6 (the in-plane symmetry-breaking crystal-field interaction) in these phase transitions, and to determine values of the magnetic parameters in the Hamiltonian implied by the magnetization and magnetoresistivity measurements.

II. MAGNETORESISTIVITY

A. Experimental details

The C_6Eu sample was made by intercalating Eu metal into a kish graphite host material.[1,2,12,17] The sample which was about $8\times0.4\times0.4$ mm^3 was mounted on a printed circuit board and the printed circuit board was then attached to a copper sample holder for thermal anchoring.[12] The whole sample holder was sealed by crushing an indium ring between the cover and the body. The magnetoresistance measurements were made with a 10-mA dc constant current source using a four-point probe method.[12]

For experiments requiring temperatures below 4.2 K, the sample was directly immersed into the liquid helium. The temperature was determined from the helium gas phase pressure by a pressure gauge. For the temperature range between 4.2 and 50 K, a special cryogenic insert which controls temperature to ±0.05 K was used for this experiment. The sample chamber was isolated from the coolant (liquid ^{4}He) by a vacuum jacket. The sample chamber was filled with helium gas to a pressure of about half an atmosphere. The vacuum jacket was also filled with a small amount of helium gas. The sample temperature was controlled by a capacitance temperature controller which was not sensitive to the magnetic field. The capacitance of the capacitance sensor near the sample was

compared with that of an adjustable capacitor in the controller and the heater current was adjusted automatically to make these two capacitances match.[12]

For temperatures below 4.2 K, a small-diameter Dewar was used for the magnetoresistance measurement. In this case, the Dewar could fit into a one-in. bore Bitter magnet, providing magnetic fields up to 23 T. When the hybrid magnet was used, magnetic fields up to 29 T were available. For temperatures between 4.2 K and 50 K, the insert was designed only for a 2-in. bore Bitter magnet which could only reach 20 T. The induced voltage deduced from $\partial B/\partial t$ was proportional to the magnetic field sweep time and was measured by sweeping the magnetic field up and down. This induced voltage must be subtracted to get the correct sample signal.[12]

B. Results of the magnetoresistivity measurements

1. Longitudinal magnetoresistance $\rho_l(H_\perp)$ with $\mathbf{H}\|\mathbf{J}\perp\hat{\mathbf{c}}$

Figure 3(a) shows the magnetic field dependence of the longitudinal magnetoresistance $\rho_l(H_\perp)$ at various fixed temperatures (4.2 K $\leq T \leq$ 26.0 K).[13] For $T \ll T_N$, the curves show that $\rho_l(H_\perp)$ decreases by about 25% when the magnetic field reaches H_{c0}, but increases by about 5% at H_{c1}. Between H_{c1} and H_{c12}, the $\rho_l(H_\perp)$ remains almost constant but decreases significantly between H_{c12} and H_{c2}, and finally $\rho_l(H_\perp)$ becomes constant above H_{c2} at low temperature. For $T \geq 15$ K, a decrease in $\rho_l(H_\perp)$ is seen above H_{c2}, with the magnitude of the slope increasing with increasing temperature. Many of these features can be understood qualitatively in terms of the previously proposed spin structure.[7] The Δ state ($H < H_{c0}$) is a "frustrated spin lattice" associated with antiferromagnetically coupled spins on a triangular lattice. For the frustrated spin configuration, large spin fluctuations occur, while for the ferrimagnetic state above H_{c0}, the spins are parallel to H and spin fluctuations are suppressed. Therefore, $\rho_l(H_\perp)$ for the ferrimagnetic state is expected to be smaller than $\rho_l(H_\perp)$ for the Δ and canted spin states because of the lower probability of spin scattering of electrons in the ferrimagnetic state, consistent with the direct calculation of the magnetoresistance of C_6Eu in zero field and in the ferrimagnetic phase.[15] For $H > H_{c2}$, the spins are aligned along the external field direction and spin fluctuations are completely suppressed. Thus, $\rho_l(H_\perp)$ has a constant low value above H_{c2}. In addition, a new weak feature appears in the $\rho_l(H_\perp)$ curves at H_{c12} between H_{c1} and H_{c2}. This feature also appears in the transverse magnetoresistance curves [see Fig. 3(b)] at low temperatures, but was not identified in the magnetization measurements.[1] The Monte Carlo simulation described in the next section shows that this newly found phase transition at H_{c12} is due to the interplanar exchange coupling and is more sensitive to the magnetoresistance than to the magnetization, as discussed below.

2. Transverse magnetoresistivity $\rho_t(H_\perp)$ with $\mathbf{H}\perp\mathbf{J}\perp\hat{\mathbf{c}}$

Figure 3(b) shows the transverse magnetoresistance $\rho_t(H_\perp)$ at various fixed temperatures (1.5 K $\leq T \leq$ 50 K).[13] The large decrease ($\sim$20%) in $\rho_t(H_\perp)$ at H_{c0} is similar but slightly smaller than that for $\rho_l(H_\perp)$. However, at the second transition field H_{c1}, the transverse resistivity $\rho_t(H_\perp)$ decreases again while $\rho_l(H_\perp)$ increases; thus, $\partial\rho_t(H_\perp)/\partial H_\perp$ and $\partial\rho_l(H_\perp)/\partial H_\perp$ have opposite signs at H_{c1} for the same orientation of the external field. The behavior of $\rho_t(H_\perp)$ for $H_{c0} < H < H_{c1}$ is also qualitatively

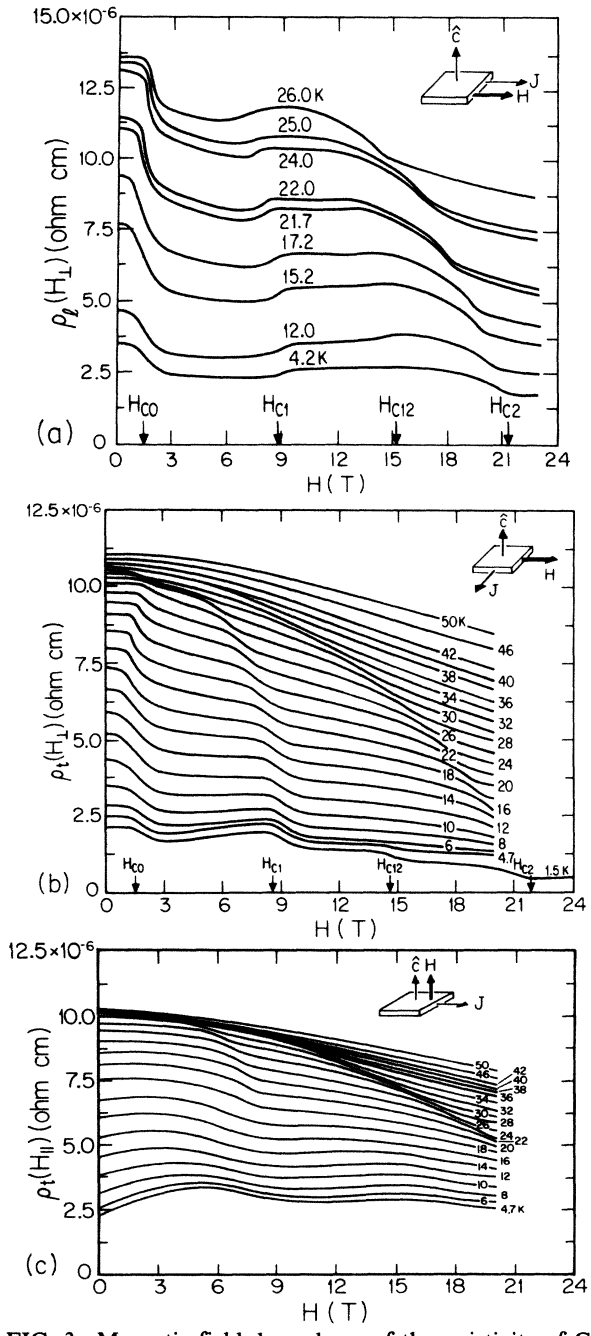

FIG. 3. Magnetic field dependence of the resistivity of C_6Eu at various fixed temperatures. The field sweep is for increasing fields. The magnetic transitions indicated by the arrows show small hysteresis (< 1 T). Three measurements with different field orientations are shown here: (a) longitudinal magnetoresistivity $\rho_l(H_\perp)$ with $\mathbf{H}\|\mathbf{J}\perp\hat{\mathbf{c}}$, (b) transverse magnetoresistivity $\rho_t(H_\perp)$ with mutually perpendicular axes $\mathbf{H}\perp\mathbf{J}\perp\hat{\mathbf{c}}$, and (c) transverse magnetoresistivity $\rho_t(H_\|)$ with $\mathbf{H}\perp\mathbf{J}$ and $\mathbf{H}\|\hat{\mathbf{c}}$.

different from $\rho_l(H_\perp)$. Specifically, $\rho_l(H_\perp)$ at low temperature is almost constant and decreases with field weakly for traces taken at higher temperatures. In contrast, $\rho_t(H_\perp)$ increases weakly with H for $T \leq 10$ K, is about field independent for $10 \leq T \leq 15$ K, and decreases weakly with field for $T \geq 15$ K. Also, for $\rho_t(H_\perp)$, the slopes of the $\rho_t(H_\perp)$ curves for $H_{c0} < H < H_{c1}$ are quite similar to those for $H_{c1} < H < H_{c2}$, except at low temperature; this is in contrast to the behavior for $\rho_l(H_\perp)$. At low temperature, $\rho_t(H_\perp)$ has a nearly constant value above H_{c2}, similar to the behavior for $\rho_l(H_\perp)$ in this field range. The weak field dependence of the resistivity observed in the ferrimagnetic phase is confirmed by the direct calculation of the magnetoresistance.[15] This theory, however, does not take account of orbital effects and does not distinguish between ρ_l and ρ_t. Since no calculations are available for the canted phase, the theory offers no explanation for the difference in behavior between ρ_l and ρ_t at H_{c1}.

The transitions in $\rho_t(H_\perp)$ are quite clear compared with those observed in the magnetization, especially at high magnetic fields and in the higher temperature ranges; the spin fluctuations in the ferrimagnetic state increase with temperature and are suppressed with field. To emphasize the magnetic transition at H_{c12}, Fig. 4 shows only the $\rho_t(H_\perp)$ curve at the lowest temperature $T = 1.5$ K, and on an expanded scale. The results of Fig. 4 clearly show a phase transition at $H_{c12} = 15$ T.

The magnetic phase diagram [see Fig. 5] has been determined from the magnetic fields and temperatures where the anomalies in $\rho_l(H_\perp)$ and $\rho_t(H_\perp)$ occur. The phase boundaries have not been determined with any accuracy in the neighborhood of 40 K. The spin arrangements shown in the figure are determined from the Monte Carlo simulation[12] described in the following sections. This phase diagram is in good agreement with the previously reported phase diagram based on the magnetization measurements[1] but the present results have higher accuracy. In addition, the present work identifies an additional phase boundary at H_{c12} between the two canted phases. The relation between the spin configurations and the resistivity changes is the subject of a separate paper.[15]

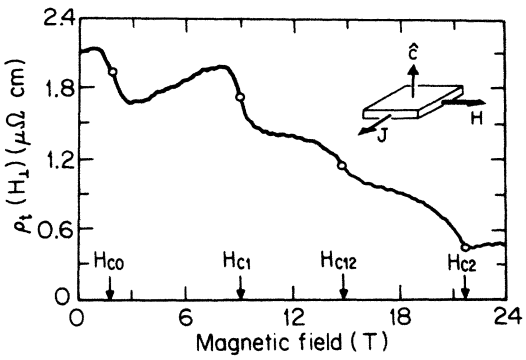

FIG. 4 Transverse magnetoresistivity $\rho_t(H_\perp)$ of C_6Eu with $\mathbf{J} \perp \mathbf{H} \perp \hat{\mathbf{c}}$ at $T = 1.5$ K, shown on an expanded scale to emphasize the transition at H_{c12}. The points indicate the fields identified with the various magnetic phase transitions.

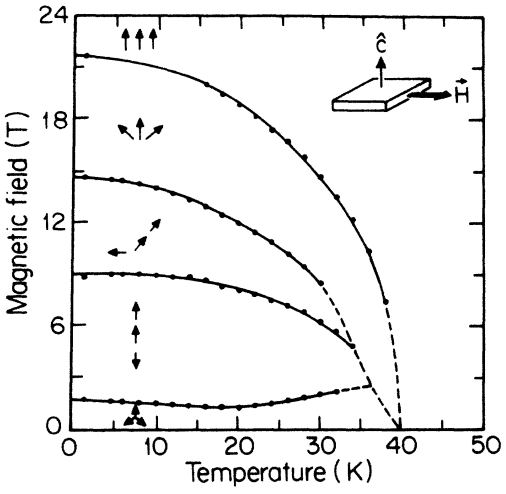

FIG. 5. Magnetic phase diagram of C_6Eu from magnetoresistivity data for $\mathbf{H} \perp \hat{\mathbf{c}}$. The phase boundaries have not been determined accurately near 40 K (dashed curves). The spin arrangements are determined from the Monte Carlo simulation.

3. *Transverse magnetoresistivity $\rho_t(H_\perp)$ with $\mathbf{J} \perp \mathbf{H} \parallel \hat{\mathbf{c}}$*

Figure 3(c) shows the field dependence of the transverse magnetoresistance with $\mathbf{H} \parallel \hat{\mathbf{c}}$. The figure shows broad and weak anomalies in the magnetoresistance $\rho_t(H_\parallel)$. For the low-temperature curves (e.g., $T \sim 4.7$ K) the anomalies occur at H_{c0} (~ 10 T), H_{c1} (~ 19 T), and H_{c2} (higher than the available fields). At 26 K, a phase transition corresponding to H_{c2} is clearly seen at 19 T and identified with the "canted"-"ferro" phase transition. The features observed for the field dependence of $\rho_t(H_\parallel)$ for $\mathbf{H} \parallel c$ axis [Fig. 3(c)] around the transition at H_{c2} are quite similar to those for $\rho_l(H_\perp)$ and $\rho_t(H_\perp)$ with $\mathbf{H} \perp c$ axis. The anomalies observed here for $\rho_t(H_\parallel)$ at lower fields (in the 6- to 9-T range) have not been reported in magnetization measurements using either pulsed field magnets or steady field magnets. In this connection, note the smoothness of the magnetization curve in Fig. 1 for $\mathbf{H} \parallel \hat{\mathbf{c}}$. A possible interpretation for these anomalies is that the Δ state goes to an intermediate canted state for the field perpendicular to the easy plane before making a transition to the ferro state. Further experiments are needed to fully specify the magnetic phase for $\mathbf{H} \parallel \hat{\mathbf{c}}$, and a theoretical spin Hamiltonian model for the magnetic phases for this field orientation is also needed.

III. MONTE CARLO SIMULATION

Monte Carlo simulation provides a powerful method for solving the statistical mechanics of complex spin Hamiltonians and thus determining the spin configurations in magnetic systems. Since C_6Eu is an XY-like magnet, its in-plane magnetic properties can be described using a 3D planar rotator model with 3D spatial dimensionality and 2D spin dimensionality. Once the Hamiltonian is specified, the simulation program calculates all the magnetic properties such as the magnetization, sus-

ceptibility, energy, heat capacity, and spin configurations. In the present work, the Metropolis importance sampling method was applied to this 3D XY system.[18] The antiferromagnetic nearest-neighbor exchange interaction results in a frustrated ground state which is very easy to obtain from a Monte Carlo simulation. The Monte Carlo simulation of the XY antiferromagnetic converges faster than that of a XY ferromagnet. Therefore, even though the C_6Eu is a 3D system with complicated magnetic interactions between spins, it is nevertheless easy to simulate the magnetic phases by the Monte Carlo method.[12]

The Monte Carlo simulation for the spin configurations in C_6Eu was based on the Hamiltonian in Eq. (1). Although the g factor (1.94) is close to 2, the possibility of a small in-plane six-fold anisotropy field H_6 due to the lattice symmetry was also considered. The Hamiltonian then becomes

$$\mathscr{H}=\mathscr{H}_0-g\mu_B S H_6 \sum_i \cos(6\theta_i) , \tag{2}$$

where $\mathscr{H}_0$ is the Hamiltonian defined in Eq. (1) and θ_i is the angle between $\mathbf{S}_i$ and $\mathbf{H}_6$.

The 3D system used for simulation includes ten layers of 30×30 triangular lattices stacked together. A total of 9000 spins was considered. One such interior layer of spins is shown in Fig. 2 for several spin configurations. The structure of the spin lattice is a hexagonal close-packed lattice with $\alpha\beta$ stacking order,[1] and free edge boundary conditions were used. The Δ state [see inset of Fig. 2(a)] is used as the initial state in each plane at $H=0$. The zero-field ground state was then generated by scanning the lattice 1000 times and applying a MCS (Monte Carlo step) to each spin in the lattice. In the actual calculations, the MCS's are applied to each spin sequentially along the lattice axes in each scan. There is no difference in the results by choosing the spin randomly for the next MCS.[19,20] In calculating physical quantities, the first 500 scans are completely neglected.[12] All arithmetically averaged physical quantities such as the magnetization and the energy (i.e., $\langle M\rangle$, $\langle M^2\rangle$, $\langle E\rangle$, $\langle E^2\rangle$, etc.) are calculated from the states generated in the last 500 scans. The reduced magnetic susceptibility $\tilde{\chi}$ and heat capacity $\tilde{C}$ are calculated using equations

$$\tilde{\chi}=(k_BT)\chi=\langle M^2\rangle-\langle M\rangle^2 , \tag{3}$$

$$\tilde{C}=(k_BT^2)C=\langle E^2\rangle-\langle E\rangle^2 . \tag{4}$$

The final zero-field state after 1000 MCS is used as the initial state of the system with a small external magnetic field $\Delta H=0.5$ T. The same Monte Carlo process is applied to determine $\langle M\rangle$, $\langle E\rangle$, $\tilde{\chi}$, and $\tilde{C}$ in the presence of an external field. Similarly, the final state of the system with field H_0 is used as the initial state of the system with field $H_0+\Delta H$, and in this way the magnetic field dependences of $\langle M\rangle$, $\langle E\rangle$, $\tilde{\chi}$, and $\tilde{C}$ are found. The calculations were performed in both increasing and decreasing magnetic fields to study hysteresis effects. Usually, increasing the temperature will cause larger fluctuations in the Monte Carlo result than increases in external magnetic field and more MCS's are needed to eliminate the fluctuations. To work out well-defined spin configurations and also to save computer time, the temperature of the system was chosen to be 0.02 K. Figure 5 shows that all the important phases occur at low temperature. On the other hand, the interesting behavior in the phase diagram above 30 K was not studied in the present work.

IV. MONTE CARLO RESULTS

To determine the role of the interplanar interaction J' and the in-plane anisotropy field H_6 in producing the observed magnetic phase transitions, the following four cases were considered in the Monte Carlo simulation: case I: $J'=0$ and $H_6=0$, case II: $J'=0$ and $H_6\neq0$, case III: $J'\neq0$ and $H_6=0$, and case IV: $J'\neq0$ and $H_6\neq0$, and the results are described below.

A. Case I: $J'=0$ and $H_6=0$

In this case, the C_6Eu system is treated as a pure two-dimensional magnetic system (the $J'=0$ approximation is valid in the high-stage limit for Eu-GIC's). From the Monte Carlo simulation for $J'=0$ and $H_6=0$ we reach two conclusions: (i) that the biquadratic and four-spin ring terms are needed to explain the $\frac{1}{3}$ moment plateau in the magnetization, and (ii) that additional interactions are necessary to explain the details of the observed magnetoresistance behavior. For a Hamiltonian without higher-order (biquadratic and four-spin) interactions, the Monte Carlo simulation shows that all spins remain lined up as the external magnetic field is increased and no magnetic phase transitions occur. In this case, the magnetization curve is quite linear until it saturates. By adding the biquadratic exchange interaction to the Hamiltonian, the spin configurations shown in Figs. 2(a), 2(b), 2(c), and 2(d) are obtained by the Monte Carlo simulation, but the magnetization curve still remains quite linear and no $\frac{1}{3}$ moment plateau appears. The Monte Carlo simulation further shows that the introduction of the four-spin exchange interaction is needed to explain the $\frac{1}{3}$ moment plateau in the magnetization curve. The spin configurations obtained from the simulation are found to be consistent with spin configurations proposed by Sakakibara and Date[1,7] and shown in the insets to Fig. 2, including the ferrimagnetic phase, where the Monte Carlo simulation shows that for $J'=0$ and $H_6=0$ all spins are exactly parallel or antiparallel to each other.

However, the spin pictures obtained with $J'=0$ and $H_6=0$ do not fully reproduce the results of the magnetoresistivity experiments, especially the observed magnetic phase transition at H_{c12} between H_{c1} and H_{c2}. Also, the transition at H_{c2} in the simulated magnetization curve is not as sharp as that observed experimentally. To achieve a better fit to the experimental results, nonvanishing values for J' and H_6 were explored.

B. Case II: $J'=0$ and $H_6\neq0$

The Monte Carlo simulation for $J'=0$ and $H_6\neq0$ shows that if H_6 is large enough ($H_6\geq500$ Oe), the canted phase will split into two different magnetic phases. One phase remains a canted phase with an angle of $\sim120°$ between nonparallel spins while the other one is the fan

phase characterized by a $\sim 60°$ angle between nonparallel spins [see Fig. 2(d)]. The new phase transition between the canted phase and the fan phase at H_{c12} appears about halfway between H_{c1} and H_{c2}. For case II, the Δ phase, the ferrimagnetic phase, and the spin-aligned paramagnetic phase spin configuration are the same as in case I. The simulated magnetization curve remains very smooth between the H_{c1} and H_{c2}, in accordance with experiment. The simulated spin picture is consistent with the observed magnetoresistivity results.

However, the H_6 field required to yield the phase transition at H_{c12} is so large that the spin configurations and transition fields of the simulation depend on the direction of the external applied magnetic field **H** relative to the easy axis $\mathbf{H}_6$. The magnetoresistivity experiments, however, show no angular in-plane dependence for the transition fields, indicating that case II does not satisfactorily account for the experimental results.

C. Case III: $J' \neq 0$ and $H_6 = 0$

Physically we know that $J' \neq 0$ for the stage-1 compound C_6Eu (see Table II). Therefore the Monte Carlo simulation for case III is of particular interest. The magnetization versus field curve obtained from the Monte Carlo simulation for case III based on the Hamiltonian in Eq. (1) is shown in Fig. 6. It is seen that although a magnetic phase transition is found at H_{c12} in the Monte Carlo simulation (see Fig. 2) the magnetization curve (Fig. 6) is still very smooth between H_{c1} and H_{c2}. The simulation shows that the phase transition at H_{c12} is not as distinct as the others, thus accounting for the fact that it was not observed in the magnetization data. The magnetization curve (Fig. 6) shows a moment equal to $\frac{1}{3}$ of the value at the high-field plateau and is in qualitative agreement with the experimental magnetization data. In carrying out the Monte Carlo simulation, the parameters of the Hamiltonian [Eq. (1)] are fitted to yield the observed magnetic transition fields H_{c0}, H_{c1}, H_{c2}, and H_{c12} in the magnetoresistivity curves. The values of the parameters obtained in this fit are listed in Table II along with the values originally proposed by Sakakibara and Date.[7] The two sets of parameters agree in all cases to within $\sim 30\%$. The value

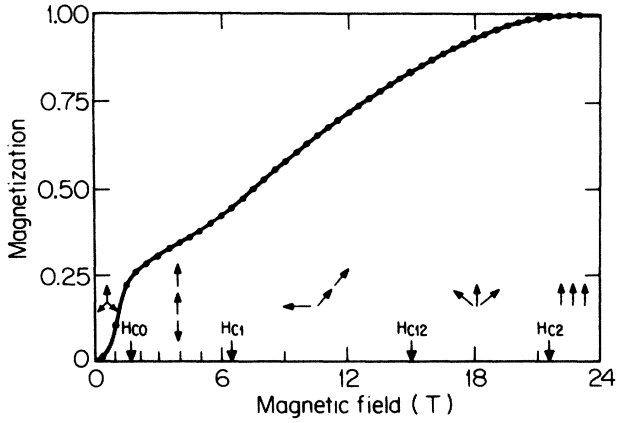

FIG. 6. Magnetization of C_6Eu versus applied magnetic field from Monte Carlo simulation based on the Hamiltonian in Eq. (1). (See Table II for values of the parameters).

of the critical fields obtained from the simulation are $H_{c0} \sim 1.5$ T, $H_{c1} \sim 6.5$ T, $H_{c12} \sim 15$ T, and $H_{c2} \sim 21.5$ T for the exchange constants listed in Table II. These values are in good agreement with the results of the magnetization measurements ($H_{c0} = 1.6$ T, $H_{c1} = 6.4$ T, and $H_{c2} = 21.5$ T). If we increase the value of KS^2, the Monte Carlo simulation shows that H_{c1} will increase and H_{c0} will decrease. With a sufficiently large KS^2 value (for example, 0.1 K), the critical field H_{c0} will be reduced to zero, the ferrimagnetic state will become the ground state, and the Δ state will no longer exist.

The simulated spin configurations for different external magnetic fields, corresponding to each of the magnetic phases are shown in Figs. 2(a) to 2(d). The spin configuration for the spin-aligned phase with the spins all along the magnetic field is not shown. The figure presents the in-plane spin orientations of a 30×30 triangular spin lattice which is one of the ten layers used to simulate the C_6Eu system. The external magnetic field is in plane but is in the upward direction of the two-dimensional net shown in the figure. The spin configurations in different layers are similar to each other. Figure 2(a) shows the spin configuration at $H = 0$ (the ground state without an external magnetic field). Two degenerate frustrated Δ spin configurations (see inset) coexist in this layer and are separated by a domain boundary.

Figure 2(b) shows the spin configuration at $H = 3$ T (the ferrimagnetic phase). One-third of the spins align approximately along the external field direction while the other spins are oriented in pairs along approximately opposite directions. We note that this configuration [Fig. 2(b)] is similar but not identical to that in the pure 2D case for $J' = 0$ (see inset) where the spins are perfectly aligned parallel or antiparallel to a given direction; for finite J' values, the parallel and antiparallel spin alignments are no longer perfect. Two degenerate spin configurations are seen in Fig. 2(b) separated by a phase boundary. These ferrimagnetic configurations result in a plateau in the magnetization curve with a moment $\frac{1}{3}$ of the saturation value, similar to the result obtained for case I.

Figure 2(c) shows a canted spin configuration at $H = 13$ T which is just below the critical field $H_{c12} = 15$ T. The canted phase shows one pair of spins making an angle close to 120° and another almost parallel pair. The canted phase is found by the Monte Carlo simulation between H_{c1} and H_{c12}.

Figure 2(d) shows a fan spin configuration at $H = 17$ T which is just above the critical field $H_{c12} = 15$ T. In the fan phase one pair of spins makes an angle of $\sim 60°$ at $H \sim 17$ T and another pair is nearly parallel; the fan phase is found between H_{c12} and H_{c2}. The value of H_{c12} (15 T) determined from the change of spin configuration from the canted phase to the fan phase is consistent with the results of the magnetoresistivity measurements (see Fig. 3). Above H_{c2} all spins are lined up along the field direction; this configuration is not shown in Fig. 2.

D. Case IV: $J' \neq 0$ and $H_6 \neq 0$

Monte Carlo simulations with H_6 equal to 1, 2, 5, 10, 100, 200, 500 Oe were performed with $J' \neq 0$ (the 3D

case). The results show that a six-fold symmetry-breaking field $H_6 \leq 500$ Oe is too small to affect the spin configurations significantly for $J' \sim 2600$ Oe (0.13 K). The simulation results do, however, show a tendency for the spins to align along the H_6 directions. The Monte Carlo calculations thus show that the interplanar interaction J' is essential for the magnetic phase transition at H_{c12} and that in-plane H_6 fields below 500 Oe will not significantly affect the nature of the magnetic phase transitions in C_6Eu.

V. CONCLUSION

The magnetic properties of C_6Eu are thus explained by a 3D XY model with a spin Hamiltonian including four-spin interactions. The exchange couplings are comparable in magnitude to those of pristine Eu metal but are physically different insofar as they involve a coupling to the graphite π-band electrons. Large changes in the resistance occur at the various magnetic phase boundaries and these anomalies are used to determine the magnetic phase diagram. Monte Carlo simulation has been used to establish the spin configurations in the various magnetic phases, and to evaluate the magnetic fields for the magnetic phase transitions as well as the values of the parameters in the magnetic Hamiltonian.

ACKNOWLEDGMENTS

The authors express their appreciation to Dr. K. Sugihara for many useful discussions and comments. The magnetoresistance experiments were done at the Francis Bitter National Magnet Laboratory (supported by the National Science Foundation) with help from Mr. L. Rubin and Dr. B. Brandt. The work at MIT was supported by the Air Force Office of Scientific Research under contract F49620-83-C-0011. S. T. Chen gratefully acknowledges support by IBM and Professor H. Suematsu and Professor Y. Yosida were supported in part by a Grant-in-Aid from the Ministry of Education of Japan.

[1]H. Suematsu, K. Ohmatsu, T. Sakakibara, M. Date, and M. Suzuki, Synth. Met. **8**, 23 (1983).

[2]M. El Makrini, D. Guérard, P. Lagrange, and A. Hérold, Physica **99B**, 481 (1980).

[3]M. Date, T. Sakakibara, K. Sugiyama, and H. Suematsu, *High Field Magnetism*, edited by M. Date (North-Holland, Amsterdam, 1983), p. 41.

[4]H. Suematsu, K. Ohmatsu, and R. Yoshizaki, Solid State Commun. **38**, 1103 (1981).

[5]G. Kaindl, J. Feldhaus, U. Ladewig, and K. H. Frank, Phys. Rev. Lett. **50**, 123 (1980).

[6]H. Suematsu, K. Ohmatsu, K. Sugiyama, T. Sakakibara, M. Motokawa, and M. Date, Solid State Commun. **40**, 241 (1981).

[7]T. Sakakibara and M. Date, J. Phys. Soc. Jpn. **53**, 3499 (1984).

[8]T. Sakakibara, J. Phys. Soc. Jpn. **53**, 3607 (1984).

[9]E. A. Harris and J. Owen, Phys. Rev. Lett. **11**, 9 (1963).

[10]D. S. Rodbell, I. S. Jacobs, and J. Owen, Phys. Rev. Lett. **11**, 10 (1963).

[11]M. Matsuura, Y. Okuda, M. Morotomi, H. Mollymoto, and M. Date, J. Phys. Soc. Jpn. **46**, 1031 (1979).

[12]S. T. Chen, Ph.D. thesis, Massachusetts Institute of Technology, 1985 (unpublished).

[13]H. Suematsu, H. Minemoto, K. Ohmatsu, Y. Yosida, S. T. Chen, G. Dresselhaus, and M. S. Dresselhaus, Synth. Met. **12**, 377 (1985).

[14]E. McRea, D. Billaud, J. F. Marêché, and A. Hérold, Physica **99B**, 489 (1980).

[15]K. Sugihara, S. T. Chen, and G. Dresselhaus, Synth. Met. **12**, 383 (1985); and unpublished.

[16]T. Sakakibara, K. Sugiyama, M. Date, and H. Suematsu, Synth. Met. **6**, 165 (1983).

[17]M. El Makrini, D. Guérard, P. Lagrange, and A. Hérold, Carbon **18**, 203 (1979).

[18]N. Metropolis, A. W. Rosenbluth, M. N. Rosenbluth, A. H. Teller, and E. Teller, J. Chem. Phys. **21**, 1087 (1953).

[19]K. Binder and D. Stauffer, *Applications of the Monte Carlo Method in Statistical Physics*, Vol. 36 of *Topics in Current Physics*, edited by K. Binder (Springer-Verlag, Berlin, 1984).

[20]K. Binder, *Monte Carlo Method in Statistical Physics*, Vol. 7 of *Topics in Current Physics*, edited by K. Binder (Springer-Verlag, Berlin, 1979).